Journal of Magnetism and Magnetic Materials 546 (2022) 168871

Contents lists available at ScienceDirect

Journal of Magnetism and Magnetic Materials

journal homepage: www.elsevier.com/locate/jmmm

Efficient spin pumping into metallic $SrVO_3$ epitaxial films

F. Macià [a,b,*], M. Mirjolet [c], J. Fontcuberta [c]

[a] Department of Condensed Matter Physics, University of Barcelona, Barcelona 08028, Spain
[b] Institute of Nanoscience and Nanotechnology (IN2UB), University of Barcelona, Barcelona 08028, Spain
[c] Institut de Ciència de Materials de Barcelona (ICMAB-CSIC), Campus UAB, Bellaterra, Catalonia 08193, Spain

ARTICLE INFO

Keywords:
Spin pumping
Magnetic damping
Spin currents
Vanadium perovskites

ABSTRACT

Spin pumping across interfaces between metallic $SrVO_3$, where V is a $3d^1$ ion, epitaxial thin films and ferromagnetic $Ni_{80}Fe_{20}$ is reported. Data shows an efficient spin pumping with a spin mixing conductance value ($g^{\uparrow\downarrow} = 11.8 \times 10^{18}$ m^{-2}) similar to that reported in metallic Vanadium but significantly larger than that measured in isoelectronic ($3d^1$) VO_2, which displays a Mott transition. Data are rationalized in terms of the relevance of density of states at the Fermi level and the relative strength of electron–electron correlations and electron-lattice coupling as toggles to tune spin-mixing conductance across interfaces.

1. Introduction

The generation of pure spin currents and the associated charge-spin and spin-charge conversion are being intensively investigated aiming at greener spintronic devices [1]. Spin-charge conversion relies essentially on spin–orbit coupling and therefore it is predicted to be larger in heavy metals. Indeed, the spin Hall angle (θ_{SH}), which is a measure of the efficiency of spin-charge conversion, has been found to roughly scale with Z^4 (Z is the atomic number) for a given d-electron count although electron filling within the 5d block largely modifies the magnitude an even the sign of it [2]. However, the experimental observation that in 3d transition metals, θ_{SH} varies systematically with 3d-orbital filling, clearly indicates a more involved scenario in which Z^4 and orbital filling both cooperate into charge-spin conversion [3]. Within this context, research on spin-charge conversion in light transition metals (3d) and its derivatives, such as transition metal oxides is emerging. For instance, it has been reported that θ_{SH} of Cr and Ni are found to be comparable (in magnitude) to Pt [4]. However, still there is no consensus on the actual values of θ_{SH} and the mechanisms behind. Another example is the case of Cr; from the comparison of θ_{SH} in YIG/Cr and YIG/Cu/Cr structures it was proposed that the larger value of θ_{SH} (orders of magnitude) observed in YIG/Cr reflects a predominant role on interfacial Rashba-Edelstein effect, rather than a bulk spin–orbit coupling [4], as earlier found in other systems (i.e YIG/graphene [5]). In the same vein, the light metallic V has been shown to display different θ_{SH} values depending on its crystallographic phase, and surprisingly enough, being as large as Pt [6].

Recently, the spin mixing conductance across interfaces between magnetic materials, such as insulating YIG [7] or $Ni_{80}Fe_{20}$ (permalloy, Py) [8] and vanadium dioxide (VO_2) has been first explored. VO_2 displays a metal–insulator transition (MIT) upon heating. In both mentioned manuscripts [7,8] the main interest was to investigate the impact of the change of resistivity of VO_2 at the MIT, on the spin pumping and the accompanying spin mixing conductance across the corresponding interfaces [9]. For instance, Safi *et al.* [7] reported that the magnetic Gilbert damping (α) in YIG increased by about a factor 2,5 (up to 2,6 $\times 10^{-4}$ in YIG/VO_2) or by a factor 1,5 (up to 6 $\times 10^{-3}$ in $Ni_{80}Fe_{20}$/VO_2) when the adjacent VO_2 layer crosses the insulator-to-metal MIT transition. Indeed, it is known that in VO_2 (rutile structure) electron–electron correlations and a Peierls transition cooperate to an electronic reconstruction that ends up in such a metal-insulator transition, where electrical resistivity changes several orders of magnitude [10–12]. When approaching the MIT from high temperature, that is from its metallic side, it is commonly assumed that the strong electron–electron correlations within the narrow 3d band, exacerbated by a structural distortion occurring at MIT, lead to the opening of a Mott gap. Although the relevance of the proximity to a MIT on spin-charge conversion is not yet known, data show that magnetic damping in the metallic state of VO_2 is larger than its insulating state, raising questions on the impact of electron–electron correlations and band reordering on spin-current injection.

Here, we report on spin pumping experiments in a single crystalline metallic oxide, $SrVO_3$ (SVO), seemingly simpler than VO_2. Indeed, and in contrast to VO_2, SVO is an excellent metal; in bulk it has a cubic perovskite structure and the $3d^1$ (V^{4+}) electronic configuration accounts for its metallic and Pauli paramagnetic character with a resistivity below ≈ 100 μΩcm at room temperature that remains metallic down to the

* Corresponding author.

https://doi.org/10.1016/j.jmmm.2021.168871
Received 7 October 2021; Received in revised form 18 November 2021; Accepted 22 November 2021
Available online 25 November 2021

lowest temperatures [13,14]. Interestingly, whereas the common wisdom was that SVO is a simple example of a correlated electronic system [15,16], recent results appear to suggest a novel scenario in which the electron-lattice coupling would dress the itinerant carriers [17]. Therefore, SVO radically differs from VO_2 and may lead to novel scenarios that may be reminiscent of polaronic spin transport [18]. Using ferromagnetic resonance spectroscopy experiments on SVO/$Ni_{80}Fe_{20}$ structures and suitable control samples we demonstrate that spin pumping into an epitaxial metallic oxide (SVO) containing light V ions is achieved. It is found that the spin mixing conductance value is one order of magnitude larger than in VO_2 and similar to metallic V. We discuss these relationships in terms of the relevance of the density of states at the Fermi level on the efficiency of spin pumping across interfaces.

2. Experimental

Epitaxial thin films of SVO were deposited on $SrTiO_3$ (STO) single crystalline substrates by pulsed laser deposition (PLD). Extensive details on growth conditions and structural, optical and electrical characterization can be found elsewhere [14,19]. Here, we shall use SVO films of thicknesses $t_{SVO} = 5$ and 15 nm, with thickness determined by the number of PLD pulses and suitable calibration. After growth, films were transferred to an e-beam evaporation chamber for room-temperature growth of a ferromagnetic layer of Py with thickness $t_{Py} = 10$ nm. Py films were also simultaneously grown on oxidized silicon wafers (SiO_x) and bare STO substrates to be used in control experiments. The final heterostructure is sketched in Fig. 2b.

The set up for ferromagnetic resonance spectroscopy (FMR) is shown in Fig. 1a. We used a vector network analyzer (VNA) in combination with a coplanar waveguide (CPW) that transforms the rf-electrical signal into an oscillatory magnetic field on the thin film's structure. Samples were mounted in flip-chip geometry on the CPW and the external static magnetic field, H_0, was applied in the sample plane and perpendicular to the oscillatory magnetic fields from the CPW. We record the rf-electrical signal transmission through the CPW as a function of external field and frequency to obtain a map of ferromagnetic resonances as shown in Fig. 1b. We varied the external magnetic field from −0.5 T to 0.5 T and the microwave frequencies from 10 MHz to 16 GHz.

3. Results

X-ray diffraction data of an illustrative SVO film indicate a single phase of fully textured material grown on STO substrates. Fig. 2a shows data for SVO (10 nm) films. The observation of the Laue fringe around the (0 0 2) SVO reflection (indicated with an arrow) assesses excellent crystalline quality of films, allows to confirm its thickness, and illustrates its planarity. In Fig. 2b we show the corresponding temperature dependent electric resistivity. As mentioned the metallic character is preserved down to the lowest temperature.

The measurement of microwave absorption—through electrical transmission in the CPW—as a function of both microwave frequency, f, and applied external magnetic field, H_0, determines the resonance frequencies and, thus, the FMR dispersion, shown in Fig. 1b. Such a dispersion relation, i.e., field versus frequency, for the case when external field is applied in the film plane is described by the Kittel equation [20]

$$f_{FMR} = \frac{\gamma}{2\pi}\sqrt{H_0\left(H_0 + 4\pi M_{eff}\right)}, \quad (1)$$

where f_{FMR} is the FMR frequency, γ is the gyromagnetic ratio ($\frac{\gamma}{2\pi} \approx 2.8$MHz/G), H_0 the applied external magnetic field, and $4\pi M_{eff} = 4\pi M_S - H_k$ the effective field given by the saturation magnetization M_S and the out-of-plane anisotropy field, H_k .

Our FMR measurements agree well with the Kittel dispersion given by Eq. (1) as shown in Fig. 1b where the 2d plot corresponds to data of a 10 nm Py thin film on SiO_x (denoted SiO_x/Py) and the red dashed line is the best fit using Eq. (1). Typical absorption lineshapes are shown as traces in the inset of Fig. 1b corresponding to frequencies of 7.5, 11 and 14 GHz. Obtained values for $4\pi M_{eff}$ are 10.55 kG for SiO_x/Py, 10.50 kOe for STO/Py and 9.5 kG for SVO/Py, indicating a slight induced out-of-plane anisotropy in the heterostructures caused by the interface SVO/Py. It is known that Py grown on SiO_x displays negligible out-of-plane anisotropy; as the measured $4\pi M_{eff}$ values for SiO_x/Py and STO/Py are very similar, we conclude that STO/Py also has a negligible anisotropy. Therefore, we take $4\pi M_s \approx 10.5$ kG (836 emu/cm^3) as the saturation magnetization value for our Py films, which is close to the value typically used for Py.

The FMR absorption lineshape (absorption as a function of external field at a fixed frequency) is usually assumed to have a symmetric Lorentzian lineshape (or asymmetric if detection is done by modulating the external field and using lock-in techniques). However, conductive samples may induce microwave eddy currents in the film and affect the lineshape symmetry [21]. We fitted the FMR absorption to a combination of symmetric and antisymmetric contributions (see traces in Fig. 1b) [22]. The full width at half maximum (FWHM) of the FMR absorption lineshapes is a measurement of the magnetization relaxation mechanisms.

Our main goal here is measuring the magneto dynamic damping and the variations caused by the SVO layers as indication of additional magnetic dissipation. We, thus, measured FMR linewidth, ΔH, as a function of microwave frequency, f, and extracted the damping parameter, α , following the relation [23]

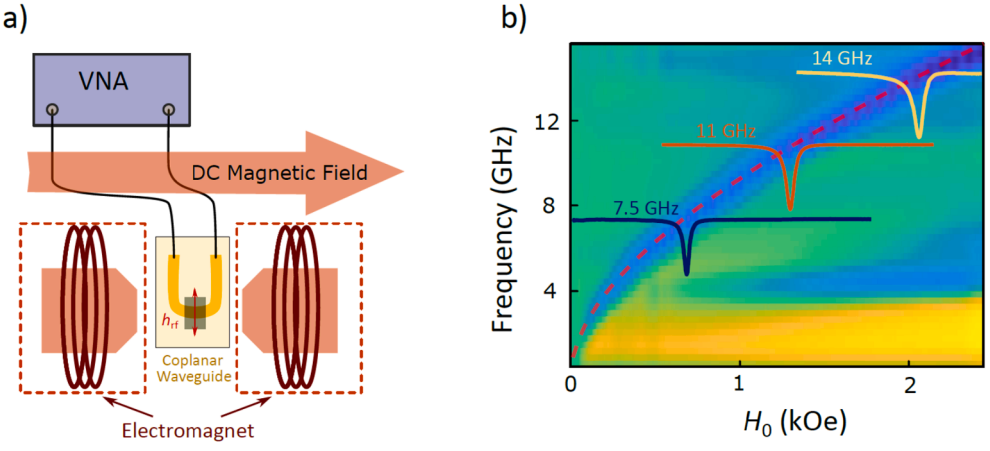

Fig. 1. a) Schematic plot of the used setup for the FMR measurement showing the critical components: a vector network analyzer (VNA) to generate and detect rf-electrical signals, a coplanar waveguide (CPW) to convert the rf-electrical signal into an oscillatory magnetic field with frequency, f, and an electromagnet to generate dc fields, H_0. b) in-plane measurement of the field versus frequency FMR dispersion relation in a 10 nm Py film grown on oxidized silicon substrate. The red dashed line corresponds to the model calculation for the FMR main peak following Eq. (1). The traces correspond to single frequency (7.5, 11 and 14 GHz) field sweeps showing FMR peaks. (For interpretation of the references to colour in this figure legend, the reader is referred to the web version of this article.)

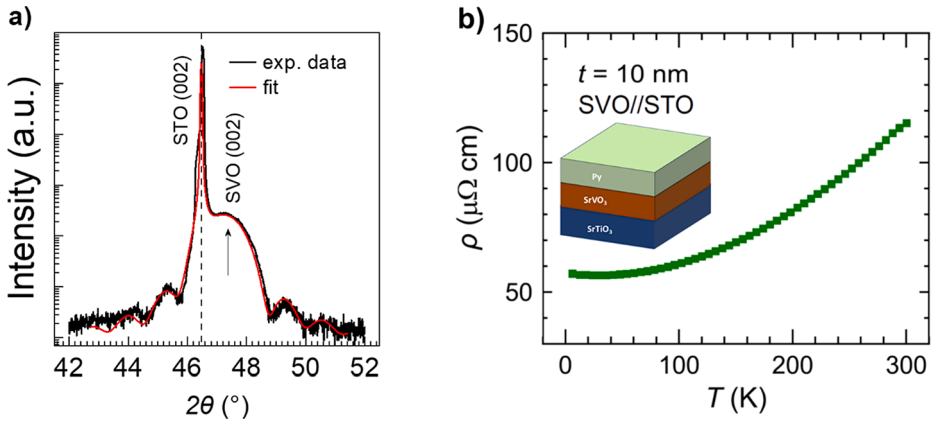

Fig. 2. a) X-ray θ-2θ diffraction pattern around the (002) reflection of the SVO (10 nm) film on STO (001). Continuous line is the fit of the Laue fringes around SVO (002) and it is used to determine the c-axis of the film and the film thickness. b) Temperature dependent resistivity of SVO (10 nm) film. Inset in b) sketches the structure of samples for spin pumping (FMR) experiments.

$$\Delta H = \frac{4\pi}{\gamma}\alpha f + \Delta H_i, \tag{2}$$

where ΔH_i is the inhomogeneous linewidth broadening, which accounts for magnetic inhomogeneities.

In presence of the SVO capping, different mechanism may contribute modifying the damping coefficient in eq. (2). Among others, magnetic reconstructions at the Py/SVO interface can modify magnetic precession. However, this interfacial effect is expected to be mostly independent of the thickness of the capping SVO layer. Experimental data (see below) clearly indicates that this is not the case. Therefore, in the following we assume that the damping induced by the SVO on the precessing Py magnetization is a measure of the spin pumping efficiency across the SVO/Py interfaces. - The spin mixing conductance (real part), $g^{\uparrow\downarrow}$, across the interface is given by

$$g^{\uparrow\downarrow} = \frac{4\pi M_S t_{Py}}{g\mu_B}\left(\alpha_{SVO/Py} - \alpha_{Py}\right), \tag{3}$$

where t_{Py} is the Py thickness, g the Landé factor ($g = 2$), μ_B , the Bohr magnetron, and $\alpha_{SVO/Py}$ and α_{Py} are the damping in SVO/Py and STO/Py layers, respectively

Fig. 3a displays the frequency dependence of the FMR linewidth, ΔH , of the 10 nm Py films grown on STO/SVO(t_{SVO}) with $t_{SVO} = 0$, 5, and 15 nm. We can see that the inhomogeneous damping is virtually identical for the three samples indicating that the growth of Py on SVO and STO does not affect Py magneto-dynamic properties—we also grew Py films on oxidized silicon wafers and obtained same values. In contrast, the slope, which is a measure of the intrinsic damping, α , is definitely larger in STO/SVO/Py than in STO/Py. We obtained damping values α of 0.0066, 0.0081 0.0087 for SVO thicknesses of 0, 5, and 15 nm (see, Fig. 3b). Data in Fig. 3a and 3b clearly demonstrate that spin pumping in Py is largely affected by the SVO capping, which thus absorbs a spin current emanating from Py.

Therefore, using Eq. (3) one can estimate the spin mixing conductance. It turns out that $g^{\uparrow\downarrow} = 9 \times 10^{18} - 11.6 \times 10^{18}\ m^{-2}$ for SVO(5 nm)/Py(10 nm) and SVO(15 nm)/Py(10 nm) respectively. The increase of $g^{\uparrow\downarrow}$ when increasing the SVO thickness but keeping the Py thickness constant (10 nm) is attributed to the fact that Eq. (3) neglects the role of the spin-diffusion length λ_{sd} within the absorbing (SVO) layer. This effect is explicitly included in Eq. (4) below [24]

$$\Delta\alpha = \frac{g\mu_B g^{\uparrow\downarrow}}{4\pi M_S t_{Py}}\left(1 - e^{-2t_{SVO}/\lambda_{sd}}\right), \tag{4}$$

where t_{SVO} is the thickness of the SVO layer.

Equation (4) is derived by considering that there is a backflow of the spin current from the SVO to the Py when the SVO is thin compared to the spin-diffusion length. The backflow spin current, I_{BP} can be described by

$$I_{BP} = I_P\left(e^{-2t_{SVO}/\lambda_{sd}}\right), \tag{5}$$

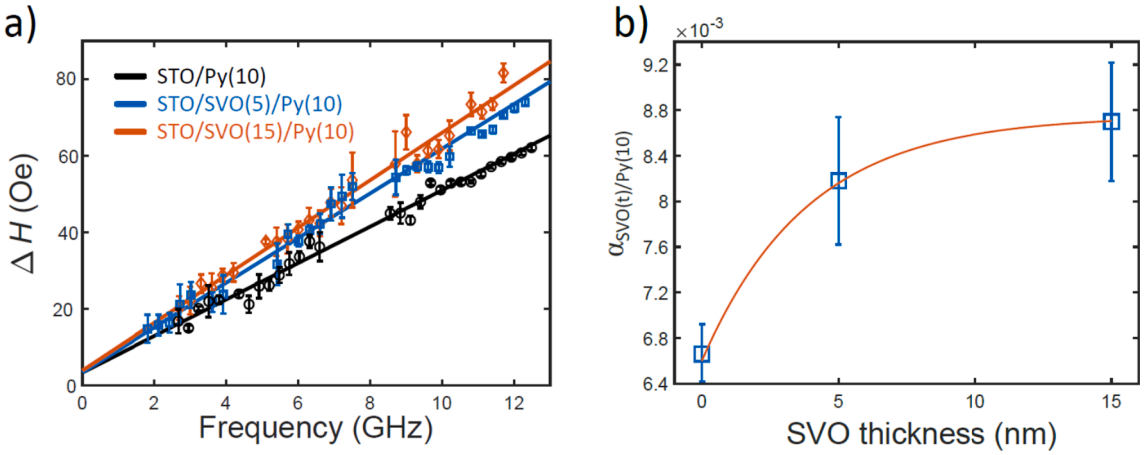

Fig. 3. a) Experimental resonance linewidth ΔH (FWHM) versus frequency of the oscillatory magnetic field for the three samples STO/SVO(t)/Py(10) with $t = 0$, 5, and 15 nm. b) Damping as a function of the SVO film thickness for the three samples shown in a). The red solid line is obtained by fitting data using Eq. (4) and. $\lambda_{sd} =$ 7.5nm is found. (For interpretation of the references to colour in this figure legend, the reader is referred to the web version of this article.)

where I_P is the pumped spin current from the Py to the SVO due to the FMR. The factor 2 appears because the effective thickness of the SVO film for the spin current making it back to Py is twice the film thickness. We, thus, have that the net spin current across the interface is then given by

$$I_S = I_P\left(1 - e^{-2t_{SVO}/\lambda_{sd}}\right), \quad (6)$$

which leads to the enhanced damping in Eq. (4).

Data in Fig. 3b can be fitted with Eq. (4) having only two independent parameters: the spin mixing conductance, $g^{\uparrow\downarrow}$, and the spin-diffusion length λ_{sd} . From the fit we obtain $g^{\uparrow\downarrow} = 5.9 \times 10^{18}$ m^{-2}, consistent with estimates made above, and $\lambda_{sd} = 7.5$nm . At this point it is worth noticing that although there are no reports on spin-diffusion length in vanadates (including VO_2) the value here obtained is about a 50% shorter than that reported in metallic V [25].

In summary, we have shown that the spin mixing conductance in SVO/Py is particularly large ($g^{\uparrow\downarrow} = 11.8 \times 10^{18}$ m^{-2}). In fact, it is about one order of magnitude larger than that reported across the YIG/VO_2 interface (8.5×10^{17}m^{-2}) when VO_2 is in its metallic phase [5]. The larger spin mixing conductance in SVO indicates that the interface is more spin-transparent; this could be related to the wider character of the conducting band in the cubic SVO than in rutile VO_2, as illustrate by the proximity to a metal–insulator transition in the latter, in which electron–electron correlations and electron-lattice coupling narrow electronic bandwidth. On the other hand, the observed spin mixing conductance compares surprisingly well with that reported in YIG/V (3.1×10^{18}m^{-2}) [2] where the electronic filling of 3d states is 3d^3 rather than 3d^1 as in the present case, suggesting that the density of states at the Fermi level and the strong electron–electron correlations there, rather than electron density, play a major role on spin mixing conductance. These conclusions can be further tested by suitable engineering of the conduction bandwidth in SVO, where epitaxial strain has been shown to be able to modulate carrier distribution within the 3d-t_{2g} manifold [26]. Finally, the proposal that carrier transport in metallic SVO displays polaronic-like features [17] may connect spin currents in vanadates to the spin polaronic transport [18]. It thus follows that intrinsic 3d metallic oxides offer opportunities for novel avenues.

Author contributions

JF and FM conceptualized, aqcuired and analyzed data. MM grew and characterized the SVO thin films. The three authors discussed the results and review edited the manuscript.

Declaration of Competing Interest

The authors declare that they have no known competing financial interests or personal relationships that could have appeared to influence the work reported in this paper.

Acknowledgements

Financial support from the Spanish Ministry of Science and Innovation, through the Severo Ochoa FUNFUTURE (CEX2019-000917-S), MAT2017-85232-R (AEI/FEDER, EU), and PID2020-118479RB-I00 projects, and from Generalitat de Catalunya (2017 SGR 1377) is acknowledged. F.M. acknowledges funding from MCIN/AEI/10.13039/501100011033 through grant number: PID2020-113024GB-100. We are thankful to Dr. J. Santiso for support on X-ray diffraction data collection.

References

[1] A. Batraas, et al., Phys. Rep. 885 (2020) 1–27.
[2] C.H. Du, Y. Pu, R. Adur, P.C. Hammel, F.Y. Yang, Phys. Rev. Lett. 112 (2014), 197201.
[3] C. Du, H. Wang, F. Yang, P.C. Hammel, Phys. Rev. B 90 (2014) 140407(R).
[4] L. Zhu, et al., App. Phys. Lett. 117 (2020), 112402.
[5] J.B.S. Mendes, et al., Phys. Rev. Lett. 115 (2015), 226601.
[6] T. Wang, et al., Sci. Rep. 7 (2017) 1306.
[7] T.S. Safi, et al., Nature Commun. 11 (2020) 476.
[8] K. Tamura, et al., AIP Adv. 11 (2021), 035120.
[9] Y. Tserkovnyak, et al., Phys. Rev. Lett 88 (2002), 117601.
[10] F.J. Morin, Phys. Rev. Lett. 3 (1959) 34.
[11] J. B. Goodenough J. Solid State Chem. **3**, 490-500 (1971).
[12] Z. Shao, et al., NPG Asia Mater. 10 (2018) 581–605.
[13] J.A. Moyer, et al., Adv. Mater. 25 (2013) 3578.
[14] M. Mirjolet, et al., Adv Funct. Materials 29 (2019) 1808432.
[15] I.H. Inoue, Phys. Rev. B 58 (1998) 437.
[16] L. Zhang, et al., Nat. Mater. 15 (2016) 204.
[17] M. Mirjolet, et al., Adv. Science 8 (2021) 2004207.
[18] S. Watanbe, et al., Nature Phys 10 (2014) 308.
[19] M. Mirjolet, et al., Adv Funct. Mater. 29 (2019) 1904238.
[20] C. Kittel, Phys. Rev. 73 (1948) 155.
[21] V. Flovik, et al., J. Appl. Phys. 117 (2015), 143902.
[22] V. Flovick, et al., J. Mag. Mag. Mat 420 (2016) 280.
[23] S.S. Kalarickal, et al., J. Appl. Phys. 99 (2006), 093909.
[24] J. Foros, et al., J. Appl. Phys. 97 (2005) 10A714.
[25] T. Wang, et al., Sci. Rep. 7 (2019) 1306.
[26] M. Mirjolet, et al., Phys. Rev. Mater. 5 (2021), 095002.